Exploiting cantilever curvature for noise reduction in atomic force microscopy

Aleksander Labuda[a] and Peter H. Grütter
Physics Department, McGill University, Montreal H3A 2T8, Canada

(Received 27 April 2010; accepted 20 September 2010; published online 20 January 2011)

Optical beam deflection is a widely used method for detecting the deflection of atomic force microscope (AFM) cantilevers. This paper presents a first order derivation for the angular detection noise density which determines the lower limit for deflection sensing. Surprisingly, the cantilever radius of curvature, commonly not considered, plays a crucial role and can be exploited to decrease angular detection noise. We demonstrate a reduction in angular detection shot noise of more than an order of magnitude on a home-built AFM with a commercial 450 μm long cantilever by exploiting the optical properties of the cantilever curvature caused by the reflective gold coating. Lastly, we demonstrate how cantilever curvature can be responsible for up to 45% of the variability in the measured sensitivity of cantilevers on commercially available AFMs. © *2011 American Institute of Physics*. [doi:10.1063/1.3503220]

I. INTRODUCTION

Optical beam deflection (OBD) method for sensing cantilever motion in atomic force microscopy was first reported in 1988 by Meyer and Amer.[1] Since then, several authors have derived the signal-to-noise ratio (SNR) of many optical assemblies used for this method of detection.[2–7] Today, most commercial atomic force microscopes use a split-diode photodetector to measure the angular changes of a light beam reflected off the backside of the cantilever. This paper revisits the first order derivation of angular detection noise in an OBD system and proposes a new paradigm for minimizing the detection noise of cantilever deflection.

In atomic force microscopy, the cantilever bending caused by forces during an experiment is usually small and thus, to first order, the cantilever deflection is considered proportional to the OBD signal—the difference in optical power (ΔP) between both sections of the split photodetector. In dynamic atomic force microscopy imaging, the SNR of OBD system is usually limited by shot noise. This is not the case in static atomic force microscopy applications such as contact imaging, lateral force imaging, and force spectroscopy, where the OBD system performs measurements in the low frequency bandwidth. The low frequency noise bandwidth is dominated by classical noise, such as pointing instabilities.[8] It can have an elaborate spectral distribution and therefore cannot be summarized by a single value such as an SNR. In this analysis, the resolution of the OBD system will be described by its angular detection noise density n_θ, in units of rad/$\sqrt{\text{Hz}}$. This describes the limit of detection of the OBD system across the full bandwidth without making any assumptions about the nature of the measurement it will be used for.

II. DERIVATION OF ANGULAR DETECTION NOISE DENSITY

The angular detection noise density n_θ is related to fluctuations in the intensity profile of the light beam used to measure the cantilever angle. These fluctuations can be measured empirically by pointing the light beam directly at the photodetector and recording the noise density of ΔP (at $\Delta P \approx 0$). This results in the optical detection noise density $n_{\Delta P}$, in units of W/$\sqrt{\text{Hz}}$. We have empirically observed that $n_{\Delta P}$ is independent of light beam diameter and detector–source distance[9] (in the limit that the photodetector is large enough and the gap between the detector sections is small enough, such that the optical power P remains constant). This fact suggests that the dominant intensity profile fluctuations are intrinsic to the light beam as it exits the optical fiber and therefore remain unaffected by the light trajectory, the optical components, or the distance between the photodetector and the optical fiber. This only holds true when the entire light path is shielded from air currents in the room.

Both $n_{\Delta P}$ and n_θ are linearly related by the first order approximation made here; therefore, any deviation $\delta(\Delta P)$ can be converted to an equivalent deviation in angle $\delta\theta$ by simple proportionality: $\delta\theta/\delta(\Delta P) = \theta_i/\Delta P_i$, where θ_i and ΔP_i are any two corresponding θ and ΔP values. It is convenient to select the maximum measurable values: $\theta_{\max}$ and $\Delta P_{\max}$. The latter is equal to the total power of the light beam $\Delta P_{\max} = P$, while $\theta_{\max}$ depends on the shape of the light beam. Solving the proportionality, in terms of noise densities, gives

$$n_\theta = \left[\frac{n_{\Delta P}(P)}{P}\right] \times \theta_{\max}, \tag{1}$$

where the dependence of $n_{\Delta P}$ on the optical power P is emphasized. The term in brackets, $n_{\Delta P}(P)/P$, is the normalized optical detection noise density, in units of $1/\sqrt{\text{Hz}}$. This describes the fraction of the light's total power P which causes fluctuations in the signal ΔP. The factor $\theta_{\max}$ represents the sensitivity of the atomic force microscope (AFM): reducing the measurable range of angles increases the sensitivity. For a fixed P, the angular detection noise is proportional to the maximum measurable angle.

[a]Electronic mail: aleks.labuda@gmail.com

For a stable light source operating at constant power, the classical noise component of $n_{\Delta P}/P$ is fixed—it is independent of the optical power P at the photodetector which may change depending on cantilever reflectivity, for example. The classical angular noise of the OBD system can only be tuned by $\theta_{\max}$, which should be made as small as possible. The exception is the shot noise component which also scales as $P^{-1/2}$. Shot noise can be reduced by increasing the optical efficiency of the OBD system—for example, by metallizing the cantilever. Whereas increasing power only reduces shot noise, both types of angular noises scale with $\theta_{\max}$. However, the wave nature of light imposes a lower limit on $\theta_{\max}$. Reaching this limit requires a thorough understanding of light propagation and diffraction.

The most accurate simple model for describing light propagation throughout the OBD system is the Gaussian beam. The complete beam shape can be described by the beam radius:[10]

$$w(z,\phi) = \frac{\lambda}{\pi\phi}\sqrt{1+\left(\frac{z\pi\phi^2}{\lambda}\right)^2}, \tag{2}$$

where z is the axial distance from the beam's focus, ϕ is the beam divergence, and λ is the wavelength of light. Figure 1(a) shows the evolution of the beam radius in the near-/midfield, where the divergent behavior is caused by the wave nature of light. At the focus, the beam radius w reaches its minimum and is called the beam waist w_o. In the near-field, the beam is collimated with a radius $\sim w_o$. In the far-field, the Gaussian beam looks like a cone of light with a half opening angle, ϕ. Mathematically, the far-field occurs when $z \gg z_R$, where z_R is the Rayleigh range, defined by $z_R = \pi w_o^2/\lambda$. The near-field and far-field are related by the fact that the product $w_o\phi = \lambda/\pi$ is constant; shrinking the beam waist w_o increases the divergence ϕ. It has been shown that placing the photodetector in the far-field maximizes SNR and renders the photodetector–cantilever distance inconsequential.[2] Equation (1) applies when this far-field condition is met.

Another important beam property is the wavefront radius of curvature, plotted in Fig. 1(b):[10]

$$R(z,\phi) = z\left[1+\left(\frac{\lambda}{\pi z\phi^2}\right)^2\right]. \tag{3}$$

Due to diffraction, the wavefront radius of a Gaussian beam varies nonmonotonically: starting with $|R| = \infty$ at the focus, the radius reaches a minimum at the Rayleigh range z_R and then grows indefinitely as it asymptotically tends toward the linear relationship $R = z$.

The metallization process in cantilever production can leave behind residual stress in the coating which may curve the cantilever. This curvature can severely modify the reflected Gaussian beam. Assuming that the cantilever thickness is uniform, the cantilever curvature along its length is perfectly circular and fully defined by its radius of curvature R_c. Upon reflection, the beam maintains its size, while its wavefront radius R undergoes a transformation given by the

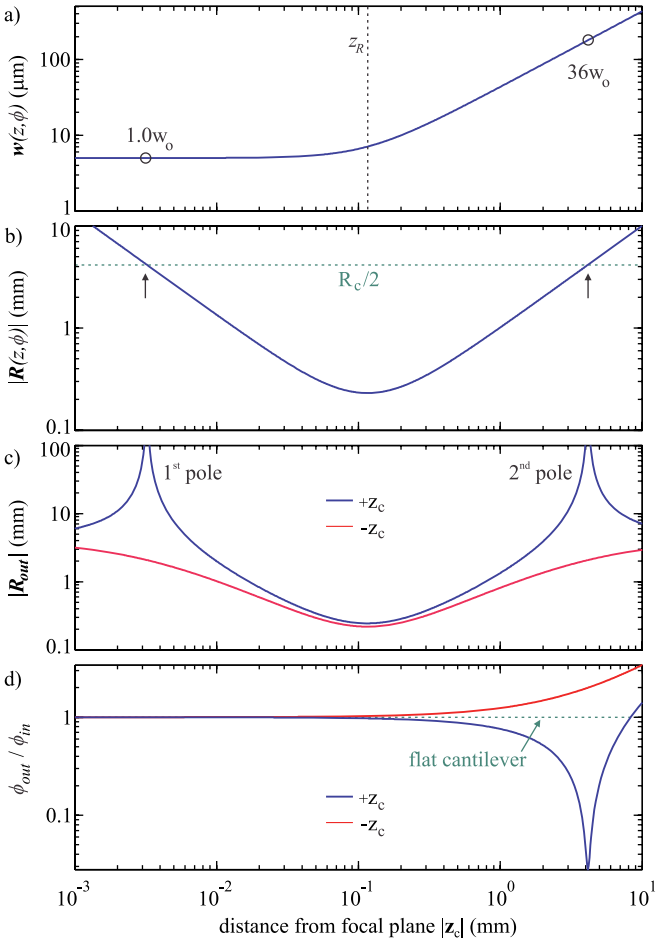

FIG. 1. (Color online) The beam divergence ($\phi = 44$ mrad) and cantilever radius ($R_c = 8.3$ mm) values used here correspond to our home-built AFM and gold-coated cantilever. All plots share the same x-axis. Negative z values are shown in red/gray, unless they overlap with positive values. (a) Beam radius and (b) magnitude of wavefront radius of incoming light beam. Dotted line: cantilever radius divided by two; this is the criterion for a collimated reflected beam. (c) Wavefront radius immediately after reflection. The two poles correspond to collimated output beams, which occur when $R_{in}^{-1} = 2R_c^{-1}$ in Eq. (4). (d) Divergence factor, which is proportional to the angular detection noise density.

formula for a spherical mirror reflection:[10]

$$R_{out}^{-1} = R_{in}^{-1} - 2R_c^{-1}. \tag{4}$$

For cantilever positions where the incoming wavefront radius R_{in} matches $R_c/2$, the outgoing beam is collimated: $|R_{out}| = \infty$. This occurs in two locations, as seen in Fig. 1(c) (unless the cantilever has a very strong curvature).

After reflection, the beam size $w_{out} = w_{in}$ and the new wavefront curvature R_{out} both define a unique Gaussian beam whose divergence ϕ_{out} can be calculated. Combining Eqs. (2) and (3) and solving gives

$$\phi_{out} = \sqrt{\frac{w_{out}^4 + R_{out}^2\frac{\lambda^2}{\pi^2}}{R_{out}^2 w_{out}^2}}. \tag{5}$$

Finally,it is this outgoing beam divergence ϕ_{out} which determines $\theta_{\max}$, used to calculate the angular noise density n_θ

in Eq. (1). A scaling factor[9] relates the two angles by

$$\theta_{\max} = \frac{\phi_{\text{out}}}{4}\sqrt{\frac{\pi}{2}}. \tag{6}$$

The six equations in this paper can be combined to calibrate the normalized optical detection noise $n_{\Delta P}/P$ into the angular detection noise n_θ for a curved cantilever positioned any distance z_c from the focus of the incoming Gaussian beam:

$$n_\theta(z_c, R_c) = \left[\frac{n_{\Delta P}}{P}\right] \times \frac{1}{4}\sqrt{\frac{\pi}{2}} \times \sqrt{\frac{w(z_c, \phi_{\text{in}})^2}{\left[R(z_c, \phi_{\text{in}})^{-1} - 2R_c^{-1}\right]^{-2}} + \frac{1}{\pi^2}\frac{\lambda^2}{w(z_c, \phi_{\text{in}})^2}},$$

where it should be reminded that ϕ_{in} is the fixed input beam divergence and therefore z_c and R_c are the only tunable variables for a typical AFM. The second component under the square root of this equation sets the lower limit of angular detection simply by virtue of diffraction. The first component represents the ray optics behavior of the reflected light beam; it is independent of λ and can be tuned by the laws governing spherical mirror reflection. Setting an appropriate values of z_c and R_c makes this component vanish, thereby minimizing detection noise.

Figure 1(d) shows the divergence factor ($\phi_{\text{out}}/\phi_{\text{in}}$) which summarizes the effect of cantilever curvature on the reflected beam. By proportionality, it is equivalent to the ratio of angular noise between a curved and a flat cantilever. For negative z_c cantilever positions, the red (gray) curve shows a steady rise in angular noise. This situation is depicted in Fig. 2(a), where the cantilever acts as a focuser and thereby increases the outgoing divergence ϕ_{out}. For positive z_c, on the blue (black) curve in Fig. 1(d), the first pole has nearly no effect on noise. This is illustrated in Fig. 2(b): collimating a beam near its focus is futile because it is already nearly collimated. At the second pole position, the beam radius has already significantly increased beyond its waist size, as shown in Fig. 2(c). Collimating the beam at that position greatly reduces the outgoing divergence because the new beam waist is now much larger upon collimation. This coincides with a large dip in the divergence factor and therefore a significant reduction in angular noise.

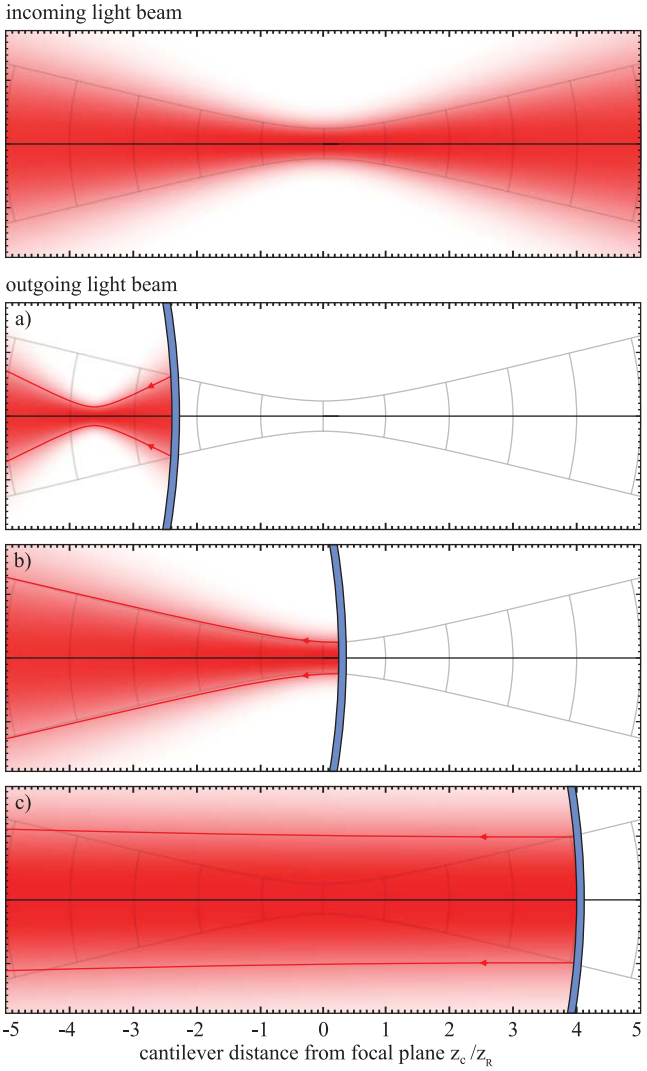

FIG. 2. (Color online) The first plot shows an incoming light beam before mounting a cantilever. In the following three plots: light gray lines represent the beam radius and wavefront curvature of the stationary incoming light beam and the arcs represent a curved cantilever at three different positions: (a) at negative z_c values, the curvature of the cantilever adds extra convergence to the incoming beam, resulting in a more strongly focused beam, with larger divergence; (b) and (c) represent both poles seen in Fig. 1(c). The outputs (b) and (c) are both collimated ($|R_{\text{out}}| = \infty$) upon reflection but in (c), the much larger beam waist results in a much smaller outgoing beam divergence.

III. RESULTS

The values used to plot Fig. 1 correspond to our particular AFM and cantilever. We experimentally verified that our beam profile deviates from Gaussian by no more than 5%. The cantilever radius $R_c = 8.3$ mm is within 'stress-free' tolerance for a 450 μm long NanoSensors™ cantilever with a Reflex™ coating (<3.5% deflection). Also, the beam divergence $\phi = 44$ mrad is within the range of many commercial AFMs; it corresponds to a focused beam diameter of 10 μm (at $\lambda = 680$ nm). For this system, moving the cantilever to $z_c = 4.2$ mm should result in a 36× reduction in outgoing beam divergence, and therefore a 36× reduction in angular detection noise.

This modeling was verified experimentally on our home-built AFM (Ref. 11) and a gold-coated cantilever with a radius of ~8.3 mm (measured with a scanning electron microscope). In Fig. 3(a), the thermal spectrum at $z_c = 0$ mm (black line) was acquired by focusing the light beam onto the cantilever. The calibration factor $\theta_{\max}$ [used to assign units of rad/$\sqrt{\text{Hz}}$ by Eq. (1)] was empirically measured by a force–distance curve on sapphire and using the cantilever geometry. In addition, a predicted value of $\theta_{\max}$ was calculated using Eqs. (2)–(5) to test the accuracy of the modeling. The inputs to this calculation were the cantilever radius of curvature (8.3 mm), the focal length of the focusing lens (25.0 mm), and the collimated beam diameter ($2w_o = 2.18$ mm) obtained from a digital photograph of the incoming light beam. The

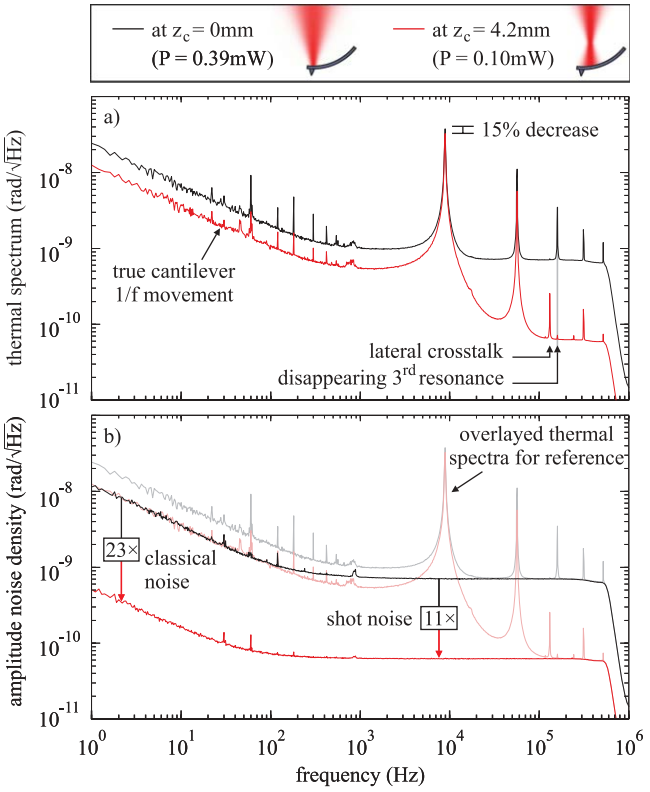

FIG. 3. (Color online) A legend is presented on top along with illustrations of the incoming light beam. The z_c coordinate of the curved cantilever [$R_c = 8.3$ mm] was changed from 0 to 4.2 mm by raising the focusing lens. (a) Thermal spectra acquired at both z_c positions. Defocusing the light beam shows a large reduction in noise because the divergence of the reflected beam was reduced by cantilever curvature. One known side-effect is that the first thermal resonance mode signal is slightly reduced (~15%) because the light beam averages a range of angles along the cantilever, resulting in a smaller effective angle measured by the light beam. Also, higher order modes see large drops in signal because their effective angles strongly depend on beam size and location on the cantilever (Ref. 12), (b) The angular detection noise n_θ was acquired in both cases by shining the light off the rigid cantilever base and matching the optical powers and calibration factors to results in (a). The classical and shot noise components of n_θ were reduced by 23× and 11×, respectively. This overshadows the ~15% signal decrease of the first resonance. At $z_c = 4.2$ mm, the fact that the $1/f$ n_θ is >20× lower than the thermal spectrum indicates that true $1/f$ cantilever movement is being measured with high precision. It should be clarified that the overlap between the $1/f$ detection noise at ($z_c = 0$ mm) and the $1/f$ cantilever movement (at $z_c = 4.2$ mm) is coincidental; the two vary between different light sources and different cantilevers. The noise around 900 Hz was caused by a computer fan—no acoustic shield was used.

measured value of$\theta_{max} = 18$ mrad, used to calibrate Fig. 3(a), exceeded the predicted value of $\theta_{max} = 14$ mrad by 29%. In other words, the angular detection noise was 29% larger than predicted by the semiempirical model presented in this paper. This discrepancy is mainly attributed to optical back reflections, stray light, and the surface quality of the cantilever, which were not considered by the model. This result illustrates why AFM users typically measure the cantilever sensitivity rather than calculate it from manufacturer's specifications.

The second thermal spectrum in Fig. 3(a) was acquired at $z_c = 4.2$ mm (red/gray line). This arrangement *seems* highly suboptimal for two reasons. First, with a larger beam diameter, the peak of the thermal spectrum is expected to drop because the light beam is not centered on the cantilever apex where the angular deflection is the largest. In fact, the first resonance peak is expected to fall 15% below the peak acquired at $z_c = 0$ mm. This percentage decreasewas calculated using theory derived by Proksch *et al.*,[13] which takes into account that a large beam averages over a range of angles along the deflected cantilever. The second disadvantage is that 76% of the optical power spills over the edge of the cantilever because of its finite width (50 μm). Despite this loss in optical power, a large reduction in angular noise can be observed in Fig. 3(a) because of the large reduction in outgoing beam divergence; now, the cantilever thermal spectrum is fully resolved above shot noise between the first and second resonances. However, it remains unclear in Fig. 3(a) what proportion of each thermal spectrum is detection noise, as opposed to actual measurable cantilever deflection. It is worth noting that thermal motion of the cantilever is considered a signal—not noise—in the characterization of an OBD system. Also, this thermal motion can be used to extract valuable information about tip–sample interactions.[14] Furthermore, even in applications where thermal motion is regarded as noise, reducing the shot noise well below the thermal noise can be highly desirable.[15]

In order to quantify the reduction in noise, the angular detection noise densities n_θ in Fig. 3(b) were acquired by reflecting the light off the rigid cantilever base, with optical powers and calibration factors matched to their respective thermal spectra from Fig. 3(a). The classical component of n_θ was reduced by 23×, which is 36% lower than the predicted value of 36×. This discrepancy is attributed to the larger relative contribution of electronic noise, optical back reflections and stray light in this situation with less reflected optical power, as well as the deviation of the reflected beam shape from Gaussian. As seen in Fig. 3(b), a reduction of only 11× was observed for the shot noise component of n_θ; the difference is mainly caused by the 76% optical power loss. Nevertheless, this loss of power is greatly outweighed by the increase in sensitivity due to the decrease in outgoing beam divergence. It is now worth reminding that the 15% loss in angular sensitivity described earlier is completely overshadowed by the 1100% lowering of shot noise and 2300% lowering in $1/f$ noise.

The drastic reduction in $1/f$ detection noise at $z_c = 4.2$ mm, in Fig. 3(b), clearly reveals that the cantilever undergoes $1/f$ movement which is now entirely resolvable above noise. This movement might be due to the viscoelastic property of the gold coating, which causes structural damping.[16] It might also be caused by $1/f$ fluctuations of the total light power, which may affect the deflection of the cantilever because of the difference in the thermal expansion coefficients of silicon and gold. Ironically, for both cases, it is the metallization of the cantilever (necessary to curve the cantilever) which causes this undesirable cantilever movement; it is not observable in uncoated cantilevers.[16]

It is clear from Fig. 3(a) that defining one value of SNR would be an oversimplification. Each cantilever flexural mode sees a different rise or drop in its angular signal because of the change in beam size and position along the cantilever.[12,17]

On the other hand, the angular detection noise density is a well-defined figure of merit which can be used to describe the precision of the OBD system before deciding on the type of measurement.

IV. UNDESIRABLE CONSEQUENCES

In as much as cantilever curvature can be exploited to reduce the detection noise of an OBD system, it can also cause a significant increase in noise for users that are unaware of it. It has been proposed that the SNR of an AFM can be maximized by focusing an elliptical light beam on the cantilever with a diameter that is 0.952× the cantilever length while loss of light is prevented by making the short-axis beam diameter smaller than the width of the cantilever.[12] This optimization rule complies with the more rudimentary theory presented here in the case of flat cantilevers: the outgoing beam divergence should be minimized by maximizing the beam diameter within the limit of the cantilever length. However, this optimization rule applies strictly to flat cantilevers, for which $\phi_{\text{out}} = \phi_{\text{in}}$. Using Eqs. (4) and (5), the outgoing beam divergence was calculated in the situation where a curved cantilever is irradiated by a focused beam of diameter equal to 0.952× the cantilever length. The radius of curvature was set to $R_c = 6.4$ mm, which is at the edge of the 'stress-free' tolerance window of the NanoSensors™ Reflex™ coating. Figure 4 shows the consequence of maximizing the incoming beam diameter on such a curved cantilever. The divergence factor $\phi_{\text{out}}/\phi_{\text{in}}$ compares the noise of a curved cantilever relative to the optimized noise of a flat one. The effect of cantilever curvature is negligible for beam diameters below ~20 μm: very strongly focused beams are impervious to moderate cantilever curvature. At a beam diameter of 60 μm, the noise sees an increase of 45% due to cantilever curvature. This explains a large part of the variability observed by AFM users in the sensitivity of commercially available cantilevers of the same model. In an Asylum Research MFP-3D™, the sensitivity of two cantilevers may differ by up to 45% by virtue of cantilever curvature alone. At large beam diameters in Fig. 4, the detrimental effect of cantilever curvature is further accentuated: an AFM optimized for 500 μm long flat cantilevers ($2w_o = 476\,\mu$m) would see an increase in divergence factor of up to 65×. Despite the benefit of a reflective coating which offers up to a threefold increase in optical power, a 500 μm long coated and curved cantilever would see at least a 20× increase in detection shot noise relative to a flat uncoated cantilever. Retrieving the minimum theoretical detection noise for 500 μm a long curved cantilever can only be achieved by reversing the situation depicted in Fig. 4(a). The incoming beam diameter must be set to 476 μm/65 = 7.3 μm and positioned at $|z_c| = 12.8$ mm. The sign of z_c depends on the sign of the radius of curvature R_c. In this case, the highly focused Gaussian beam will have expanded up to a beam diameter of 476 μm at the cantilever; then, the reflected beam will be collimated due to the cantilever curvature. This situation would restore the theoretical minimum in outgoing beam divergence and angular detection noise.

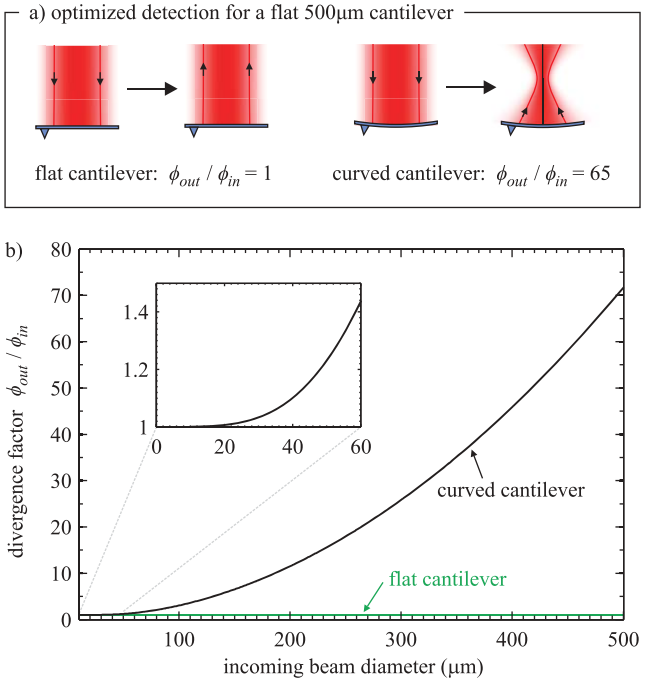

FIG. 4. (Color online) (a) An illustration demonstrates the effects of cantilever curvature on the reflected beam divergence ϕ_{out} in an AFM optimized for the detection of 500 μm flat cantilevers. Optimum performance is obtained on flat cantilevers if the beam diameter is 0.952× the cantilever length (Ref. 12). The divergence factor $\phi_{\text{out}}/\phi_{\text{in}}$, which is inversely proportional to sensitivity, represents the increase in detection noise caused by cantilever curvature. The radius of curvature was selected at the edge of the tolerance window set by NanoSensors™: $R_c = 6.4$ mm. A flat cantilever does not change the divergence of the reflected beam, in which case $\phi_{\text{out}}/\phi_{\text{in}} = 1$. A curved cantilever focuses the incoming light beam and increases the divergence, and detection noise, by 65×. (b) For generality, the same result is plotted as a function of beam diameter and applies to all cantilever sizes. Cantilever curvature has negligible effects on the outgoing divergence of light beams with diameters below 20 μm. At a diameter of 60 μm, cantilever curvature may increase the noise by up to 45% for the same model cantilever. At a beam diameter of 500 μm, a variability of up to 7200% in noise may exist due to cantilever curvature. The data here were calculated for a light beam with an 850 nm wavelength; the effects of curvature are stronger for smaller wavelengths.

V. CONCLUSION

In conclusion, the angular detection noise density n_θ of an optical beam deflection system scales with outgoing beam divergence (to first order) with an additional power gain factor $P^{-1/2}$ for the shot noise component. Cantilever curvature has a strong impact on n_θ; it can greatly enhance or reduce n_θ and therefore should not be neglected. Optimizing the cantilever distance from the light beam's focus can substantially reduce n_θ, even in commercial AFMs with commercially available cantilevers. Conversely, cantilever curvature can increase n_θ, even in the typical situation where the light beam is focused onto the cantilever. The large variation seen in the measured noise density of cantilevers of the same model can be attributed to this phenomenon. Two 500 μm long coated cantilevers with radii of curvature within the manufacturers 'stress-free' tolerance may differ in detection noise by up to 65× in an AFM optimized for the detection of flat 500 μm long cantilevers.

ACKNOWLEDGMENTS

We thank Roland Bennewitz for supervising the design and development of the AFM which led to this paper and Robert Gagnon for help with curving cantilevers. We acknowledge Mark Sutton, William Paul, Kei Kobayashi, Daniel Kiracofe, and Jeffrey Bates for valuable input on the report. We also thank Mario Viani, Deron Walters, and Jason Cleveland at Asylum Research for stimulating discussions. Lastly, we thank the anonymous referee for helpful suggestions improving this manuscript. This work was funded by Natural Sciences and Engineering Research Council of Canada (NSERC) and Le Fonds Québécois de la Recherche sur la Nature et les Technologies (FQRNT).

[1]G. Meyer and N. M. Amer, Appl. Phys. Lett. **53**, 1045 (1988).
[2]C. A. J. Putman, B. G. De Grooth, N. F. Van Hulst, and J. Greve, J. Appl. Phys. **72**, 6 (1992).
[3]T. Fukuma, M. Kimura, K. Kobayashi, K. Matsushige, and H. Yamada, Rev. Sci. Instrum. **76**, 053704 (2005).
[4]T. E. Schaffer and P. K. Hansma, J. Appl. Phys. **84**, 4661 (1998).
[5]A. Garcia-Valenzuela, J. Appl. Phys. **82**, 985 (1997).
[6]T. E. Schaffer, J. Appl. Phys. **91**, 4739 (2002).
[7]T. Fukuma and S. P. Jarvis, Rev. Sci. Instrum. **77**, 043701 (2006).
[8]T. E. Schäffer, in *Scanning Probe Microscopy Techniques*, Applied Scanning Probe Methods V, edited by B. Bhushan, H. Fuchs, and S. Kawata (Springer, New York, 2007), pp. 51–74.
[9]See supplementary material at http://dx.doi.org/10.1063/1.3503220 for supporting data.
[10]M. C. Teich and B. E. A. Saleh, *Fundamentals of Photonics* (Wiley, New York, 1991).
[11]A. Labuda, W. Paul, B. Pietrobon, R. B. Lennox, P. H. Grütter, and R. Bennewitz, Rev. Sci. Instrum. **81**, 083701 (2010).
[12]T. E. Schaffer and H. Fuchs, J. Appl. Phys. **97**, 083524 (2005).
[13]R. Proksch, T. E. Schäffer, J. P. Cleveland, R. C. Callahan, and M. B. Viani, Nanotechnology **15**, 1344 (2004).
[14]J. P. Cleveland, T. E. Schäffer, and P. K. Hansma, Phys. Rev. B **52**, R8692 (1995).
[15]K. Kobayashi, H. Yamada, and K. Matsushige, Rev. Sci. Instrum. **80**, 043708 (2009).
[16]P. Paolino and L. Bellon, Nanotechnology **20**, 405705 (2009).
[17]T. E. Schaffer, Nanotechnology **16**, 664 (2005).